Sparse innervation and local heterogeneity in the vibrissal corticostriatal projection

Abbreviated title : Functional somatosensory corticostriatal connectivity

Authors and affiliations:

Kenza Amroune[1], Lorenzo Fontolan[2], Agnès Baude[1], David Robbe[2] and Ingrid Bureau[1]*

[1] Aix-Marseille Université, INSERM, INMED, Marseille, 13009, France

[2] Aix-Marseille Université, INSERM, INMED, Turing Centre for Living Systems, Marseille, 13009, France

corresponding author email address: ingrid.bureau@inserm.fr

Abstract

The density and overlap of cortical axons in the dorsolateral striatum (DLS) have suggested that striatal neurons integrate widespread information from cortical regions that are functionally related. However, in vivo, DLS neuronal responses to sensory stimuli have shown unexpectedly high selectivity, raising questions about the actual degree of input convergence of functional corticostriatal projection on individual striatal cells. Here, we investigated this question by focusing on the projections from different whisker cortical columns, as they overlap in the striatum and are co-active during behavior. Using *ex vivo* patch-clamp recordings in the DLS and glutamate uncaging for focal stimulations in the barrel cortex, we were able to map the location of presynaptic neurons to individual striatal projection neurons (SPNs). We found that each SPN was innervated by cells located in a small number of whisker cortical columns scattered across the barrel field in the slice. Connectivity of single SPNs with cortical neurons was thus highly discontinuous horizontally, despite the presence of more potential connections. Moreover, connectivity patterns were specific to each cell, with neighboring SPNs sharing few common clusters of presynaptic cells in the cortex. Despite this sparse and distinct innervation of individual SPNs, the projection was topographically organized at the population level. Finally, we found similar innervation patterns for D1- and D2-type SPNs, but observed differences in synaptic strength in their connections with certain cortical layers, notably the associative layer 2/3. Our results suggest that the high convergence of somatosensory inputs to the striatum, enabled by diffuse and overlapping cortical innervation, is accomplished through sparse yet complementary connectivity to individual SPNs.

Introduction

The dorsolateral striatum receives dense glutamatergic innervation from all sensory cortical areas. Its presumed function is to monitor the animal's ongoing sensory information, contributing to the modulation of sensory-guided behaviors and the learning of voluntary tasks (Pennartz et al., 2009; Znamenskiy and Zador, 2013; Sippy et al., 2015; Robbe, 2018). The observations that cortical neurons are overabundant compared to striatal projection neurons (SPN) (Oorschot 1996), that axonal projections originating from functionally linked cortical regions overlap in the striatum (Flaherty and Graybiel, 1991; Alloway et al., 1999; Wright et al., 1999; Hooks et al., 2018) and that synaptic glutamatergic inputs must overcome strong feedforward inhibition (Mallet et al., 2005; Pidoux et al., 2011), have led to the idea that striatal neurons integrate dense and broad cortical inputs. In fact, studies examining the density of axonal boutons relative to the single cell dendritic spines have predicted that several thousand cortical neurons could potentially connect every SPN if synapses were formed promiscuously (Kincaid et al., 1998). However if synapses were formed in a selective manner, this would reduce the degree of convergence of cortical input onto individual SPNs and potentially increase the heterogeneity of inputs between SPNs (Kincaid et al., 1998), a scenario with important implications for how cortical information is integrated in the striatum. These alternative connectivity models schematized in Fig. 1 remained to be tested functionally.

Here, we investigated this question at the level of the projections originating from the barrel field in the mouse primary somatosensory cortex (S1) and targeting the SPNs. Vibrissal information is transmitted to the cortical columns of S1 through parallel sensory channels, each corresponding to an individual whisker (reviewed in Adibi 2019). In S1, layer 4 contains optically dense, barrel-shaped structures whose organization mirrors the spatial arrangement of whiskers on the snout. This feature provides a framework for studying neuronal connectivity in relation to the whisker cortical columns *ex vivo*. However, this model has not yet been used to examine connectivity within the functional vibrissal corticostriatal projections, leaving the degree of input convergence in this pathway unclear. On the one hand, axons of neurons located in different whisker cortical columns overlap heavily in the dorsal striatum, suggesting that SPNs could receive dense and broad vibrissal cortical input (Wright et al., 1999; Alloway et al., 2000). On the other hand, cell activity evoked by whisker deflection showed notable heterogeneity in the DLS: neurons were either tuned to multiple whiskers, selective to a single whisker, or yet non-responsive (Carelli and West, 1991; Pidoux et al., 2011). These observations prompted us to

58 investigate whether the vibrissal innervation of SPNs violated Peters' rule stating that connectivity is
59 proportional to the overlap of axons and dendrites (Peters, 1979; Braitenberg and Schüz, 1998).

60 SPNs comprise two main populations, defined by their projection targets and expression of dopamine
61 receptors: D1 receptors in the direct pathway and D2 receptors in the indirect pathway (Smith et al.,
62 1998; Kravitz et al., 2010) (neurons are hereafter referred to as D1 and D2 SPNs). Electrophysiological
63 studies have found that inputs received by D1 SPNs were stronger than those received by D2 SPNs, both
64 *in vivo* and *ex vivo* (Reig and Silberberg, 2014 ; Filipović et al., 2019 ; Kress et al., 2013 ; Parker et al.,
65 2016). These observations may indicate that inputs converge to different degrees to D1 and to D2 SPNs.

66 To investigate the connectivity and input convergence on SPNs, we used a functional mapping technique
67 that combines patch-clamp recordings and laser scanning photostimulation (LSPS) with glutamate
68 uncaging on a novel slice preparation, which preserved the organization of the vibrissal corticostriatal
69 projections, from the superficial layers of the barrel cortex to the DLS. LSPS enabled precise mapping of
70 corticostriatal functional connectivity by identifying cortical sites where stimulation evoked synaptic
71 currents in the recorded SPNs, thereby localizing the cell bodies of their presynaptic neurons. This
72 approach allowed us to determine both the cortical column and layer of origin within the barrel field in
73 the slice for each SPN input. We found overall discrete innervations, as presynaptic neurons were
74 thinly-scattered across the barrel field, or present in a single cortical column. SPNs located nearby in the
75 same slice had distinct patterns of innervation, suggesting that connections on each SPN were fewer
76 than the local potential connections. No difference was found between the innervation patterns of D1
77 and D2 SPNs, but the strength of their connections with certain layers differed.

78 Results

79 A novel preparation for investigating functionally the organization of projections from the barrel 80 cortex to individual SPNs in the DLS

81 To investigate the spatial organization of sensory projections to SPNs, we have developed a parasagittal
82 somatosensory corticostriatal slice, which contained ~ 8 whisker barrels (Methods; Fig. 2A and
83 Supplemental Fig. 1A). Biocytin-labeled projections extended from the top of the barrel cortex to the
84 DLS (Fig. 2A,B). To further validate the angles used in the preparation, we virtually re-sectioned a brain
85 from the Allen Mouse Connectivity Atlas in which pyramidal cells of the barrel cortex had been labeled
86 *in vivo* (i.e., prior to slicing; Supplemental Fig. 1B). Cortical axons extended into the striatum in a similar
87 manner in both the reconstituted and acute slices (compare Fig. 2A and Supplemental Fig. 1B),

supporting the idea that projections from the present cortical columns targeting the recorded striatal region were largely preserved in the acute slice. Animals were Drd1a-tdTomato hemizygous mice in which D1 receptor expressing neurons were labeled. $D1^+$ and $D1^-$ ($D2^+$) SPNs were recorded in the whole-cell voltage–clamp configuration (n = 101 cells, N = 54 mice). Simultaneously, an ultraviolet laser beam was directed at every site of a 29 x 16 pixel grid (2.1 × 1.1 mm, 75 µm spacing) to uncage glutamate over the barrel cortex, excite cortical neurons, and thereby reveal cells presynaptic to the recorded SPN (Fig. 2C,D). When glutamate was uncaged on an excitatory cortical neuron innervating the recorded SPN, it elicited short-lived excitatory postsynaptic currents (EPSCs; < 50 ms duration) (Fig. 2D). We and others have shown that only subthreshold synaptic events are elicited with this method, implying that the evoked EPSCs are mono-synaptic and that feedforward inhibition is prevented (Shepherd et al., 2003; Bureau et al., 2008). In fact, glutamate uncaging excited cortical neurons above their firing threshold at a maximal distance of 75 µm from their cell body (Fig. 1E; Supplemental Fig. 2A), on 2.8 ± 0.3 sites of the LSPS grid (mean ± sem; L5 pyramidal cells, n = 40; 75 µm spacing grid; see Methods), consistent with a direct (i.e., non synaptic) and nearly somatic excitation (data per cell type in the Methods and Supplemental Fig. 2). Thus, the sites where LSPS evoked EPSCs in SPNs contained or were adjacent to the cell bodies of cortical neurons that were directly connected to the recorded cell. These sites are hereafter referred to as “connected sites”. EPSCs had small amplitudes, 40 ± 1 pA (n = 550). Based on known amplitudes of spontaneous and miniature EPSCs in SPNs (10-20 pA on average; Kreitzer and Malenka, 2007; Cepeda et al., 2008; Dehorter et al., 2011; Peixoto et al., 2016), this finding is consistent with the presence of only one or a few presynaptic cells (≤ 5) at each connected site of the map.

For each SPN, an input map was assembled from the excitatory response evoked at the uncaging sites of the LSPS grid (Fig. 2D, top). From this input map, a binary map was derived which reported the presence or lack of evoked EPSC, referred to as “connectivity map”. We first analyzed the ensemble of connectivity maps to characterize the global organization of the projections from the barrel field in the slice and checked that their properties were consistent with those described by anatomical studies (Fig. 2F). When all SPN connectivity maps were superimposed and overlaid on the barrel cortex (see Methods; Fig. 2F), the connected sites principally highlighted the layer (L) 5a. Indeed, ~ 65 % of all SPNs received input from this layer (Fig. 2G). Responses were elicited less frequently when stimulations were in L4, L5b, L2/3 and in L6. We found that 50 % of L5a cells fired action potentials when stimulations were at the bottom of L4, indicating that a fraction of the relatively high connectivity rate seen at the bottom

119 of L4 was in fact with nearby L5a pyramidal cells (Fig. 2E; Supplemental Fig. 2A). In contrast, photo-
120 stimulations in L2/3 never elicited the firing of L5a cells (n = 11; Fig. 2E), indicating that all EPSCs evoked
121 by stimulations in these superficial layers arose from direct synaptic connections between L2/3
122 pyramidal cells and SPNs. EPSCs evoked with stimulations in L2/3 to L5b had similar amplitudes (Fig. 2H),
123 suggesting that L5a dominance over these other layers is primarily due to a higher likelihood of SPNs
124 being connected to it, rather than to stronger synaptic inputs. However, L6-EPSCs were smaller
125 compared to L5a and L5b-EPSCs (Kruskal-Wallis, H(4) = 22.8, p = 0.0001; Dunn post-hoc test and Šidák
126 correction, p = 0.0001 and 0.034; Fig. 2H). These observations are aligned with the anatomical studies
127 which have identified L5a as the primary, although not exclusive, source of cortical innervation in the
128 DLS (Wise and Jones, 1977; Cowan and Wilson, 1994; Wall et al., 2013).

129 In the superimposed connectivity maps, the ensemble of connected sites observed across recordings
130 formed a band in the barrel cortex that was larger than the region in the DLS containing the recorded
131 SPNs (2.5 mm vs. 1 mm, Fig. 2F). An opposite asymmetry was observed when analyzing the striatal
132 region connected to individual cortical columns: sites within a single cortical column (~ 150 µm in this
133 preparation) were connected to SPNs distributed across a larger striatal region, spanning about 600 µm
134 (Fig. 2I). These two asymmetric relationships (converging vs. diverging), summarized in Fig. 2J, implied
135 that functional projections from adjacent cortical columns overlapped in the DLS, which is consistent
136 with their known anatomy (Wright et al., 1999; Alloway et al., 2000; Hooks et al., 2018). Thus,
137 projections from the cortical columns in the slice overlapped in the striatum, which allowed us to
138 investigate the degree of convergence of whisker cortical inputs onto individual SPNs.

139 **Low convergence of projections from the barrel cortex to individual SPNs in the DLS**

140 To investigate the number and position of whisker cortical columns from which individual SPNs received
141 synaptic inputs, each connectivity map was collapsed along its vertical axis and the horizontal
142 distribution of connected sites was characterized using the following metrics (Fig. 3A): 1- the input field,
143 or the overall region within the barrel field in the slice from which an SPN receives inputs. Its width is
144 the distance between the SPN most distant connected sites.; 2- the cluster, a region in the collapsed
145 connectivity map constituted of adjacent connected sites; 3- the cortical column, or its proxy: 1 to 2
146 adjacent connected sites in the collapsed connectivity map (i.e. 75-150 µm width). The connected sites
147 were organized in 1 to 6 clusters, 1.9 ± 0.1 on average in the input fields (Fig. 3B). Typically, the width of
148 clusters was about one cortical column (171 ± 7 µm) and it rarely exceeded two adjacent columns (Fig.
149 3C). Finally, SPNs were innervated by cells distributed in close to 3 columns (2.7 ± 0.2), though some

150 SPNs with several clusters (54 %) were innervated by as many as eight columns (Fig. 3D). The distance
151 between clusters was 75 to 900 µm, 265 ± 28 µm on average (n = 55; Fig. 3C). Thus, SPNs could receive
152 inputs from clusters of cortical cells separated by substantial connectivity gaps, often spanning several
153 columns. Heterogeneous spacing and number of clusters contributed to the variability of the input fields
154 width, which ranged between 0.075 and 1.6 mm (average, 535 ± 42 µm; Fig. 3E). Strikingly, regions
155 lacking evoked synaptic responses (i.e., connectivity gaps) made up an average of 45 % of the length of
156 input fields with multiple clusters (maps collapsed along the vertical axis; Fig. 3F, bottom). Moreover,
157 the number of clusters was not increased proportionally in very large input fields, > 1.4 mm, in which
158 connectivity gaps amounted to more than 50 % of space in the horizontal axis (Fig. 3F, bottom).
159 Altogether, these findings suggest a connectivity pattern characterized by a few small patches of
160 presynaptic cortical cells scattered across the axis of barrels.

161 It could be that small input fields that contained a single cortical column (75-150 µm) were obtained
162 when recordings were performed on the edges of the striatal region with cortical innervation in the
163 slice. Contrary to this hypothesis, we found that SPNs with small input fields and those with broader
164 ones were intermingled along the horizontal axis in the striatum (open and solid symbols in Fig. 3G,
165 respectively). In fact, the width of the input fields remained relatively constant across SPN positions in
166 the slice (Fig. 3G, top; Spearman correlation coefficient, R = 0.05, p = 0.61). This suggests that the
167 position of our recordings did not impact the SPN input fields. Furthermore, SPNs receiving input from a
168 single column were often located in slices where other cells received input from multiple ones (Fig. 3D),
169 reinforcing that the low functional connectivity with barrel columns in the slice was genuine in these
170 cases.

171 Next, we investigated these connectivity patterns along their vertical axis. Individual SPNs had
172 connected sites distributed in 2.4 ± 0.1 cortical layers on average (2.9 ± 0.1 for SPNs with several
173 clusters). But these sites were not necessarily vertically aligned within a cortical column (examples in Fig.
174 2D and 3A). In fact, in 55 % of the cases, a column of the barrel field innervated an SPN through
175 projections from a single cortical layer. This suggests that neurons projecting to an SPN are dispersed in
176 the barrel cortex in such a way that the transmitted inputs may originate from distinct layers as well as
177 from different whisker cortical columns. Our findings are summarized in Fig. 3H, with schematics of the
178 average and principal connectivity patterns.

179

180 **Individual SPNs have unique innervation**

181 The above analysis has revealed great heterogeneity between SPN innervations. We then investigated
182 whether innervations were more similar when SPNs were close to each other. To address this question,
183 we compared the connectivity patterns of SPNs recorded in the same slice (Fig. 4A). First, we observed
184 that the majority of SPN pairs had their input fields overlapping in the barrel cortex (n = 70; Fig. 4B). The
185 ratio was the highest, 77 %, for SPNs that were neighbors in the striatum (< 100 µm, n = 33), but
186 remained above 50 % for cell distances of 400-500 µm. We next examined to what extent the connected
187 sites were shared or vertically aligned between the connectivity maps. In contrast to input fields,
188 alignment or overlap of connected sites was only observed when SPNs were less than 300 µm apart (Fig.
189 4B,C). Moreover, this concerned only a small fraction of the pair's connected sites: when SPNs were less
190 than 100 µm apart, only 18 ± 2 % of the connected sites in the two connectivity maps were vertically
191 aligned (Fig. 4C) and 7.7 ± 1.6 % of them overlapped (Fig. 4D). Overall, these results indicate that DLS
192 SPNs could receive inputs from the same domain in the barrel cortex and yet have patterns of cortical
193 innervation without or little redundancy. They support a connectivity model in which synaptic
194 connections on each SPNs are sparser than the potential connections, and with significant heterogeneity
195 between SPNs in terms of their whisker-related cortical inputs.

196 **Topographic organization of SPN functional vibrissal innervation**

197 The sparse innervation patterns, with limited similarity among neighboring SPNs, may seem inconsistent
198 with the known topographic organization of somatosensory corticostriatal projections. To examine the
199 global organization of functional projections in our preparation, we superimposed the connectivity maps
200 of SPNs and labeled the connected sites based on the SPN's positions in the striatum (Fig. 5A). SPNs
201 located laterally/medially in the dorsal striatum had an input field whose connectivity center of mass
202 (CM, see Methods) was in the lateral/medial part of the barrel cortex (Fig. 5A,B). Thus, the functional
203 projections from the barrel cortex were topographically organized in the DLS, consistent with anatomy
204 (Flaherty and Graybiel, 1991; Alloway et al., 1999; Wright et al., 1999; Hooks et al., 2018). Given the
205 orientation of the slice (Supplemental Fig. 1A), a shift of the connectivity CM on the horizontal axis of
206 the barrel field corresponded principally to a shift between whisker arcs (e.g. E1 to E8 barrel). The
207 connectivity CMs of two adjacent SPNs could be 1 mm apart in the barrel cortex (Fig. 5B), indicating that
208 the topographic organization was not as precise as for intracortical projections (Shepherd and Svoboda,
209 2005; Erlandson et al., 2015). This finding, together with previous analyses, supports a connectivity

210 model that falls between the two illustrated in the middle and right panels of Fig. 1 (selective, broad and
211 loosely topographic).

212 The EPSC amplitudes were heterogeneous within each input map (Fig. 5C; ex Fig. 2D). To test the
213 hypothesis of a topographic organization influencing synaptic strength, we examined whether strong
214 connections were associated with presynaptic cells located close to the connectivity CM. If such an
215 organization of synaptic strengths existed, we would expect it to improve the correlation between the
216 CM of synaptic input maps and SPN positions. However, we found nearly identical correlations whether
217 taking the connectivity CM or the synaptic input CM, which is based on the connectivity pattern
218 weighted by EPSC amplitudes (see Methods; R = 0.60 vs. 0.62; F(1) = 115.08, p = 0.98, ANCOVA; Fig. 5D).
219 While residuals from the correlation curve tended to be smaller using synaptic input CMs, the difference
220 was not statistically significant (- 9 ± 7 µm, p = 0.084, Wilcoxon, SPNs with >1 cluster). This was because
221 synaptic input CMs were only slightly shifted from the connectivity CMs, by 45 ± 5 µm for SPNs with two
222 or more clusters (Fig. 5D). These findings indicate that EPSC amplitudes showed no consistent pattern
223 relative to the connectivity CM of the input field. This confirms the connectivity patterns as principal
224 determinants of the topographic organization of somatosensory corticostriatal projections.

225 Finally, given that previous studies have revealed that responses of some striatal neurons exhibited
226 strong selectivity for specific whiskers *in vivo* (Carelli and West, 1991; Pidoux et al., 2011), we
227 investigated whether, in cases where SPNs were innervated by multiple clusters, one cluster might
228 dominate the others. Comparing the sum of EPSCs corresponding to clusters, we found substantial
229 variability, with the strongest cluster providing input that was 1.12 to 55 times greater than other
230 clusters within the input field (× 6.8 ± 1.4 on average; Fig. 5E). Thus, connectivity patterns with multiple
231 clusters may still permit some SPNs to have a preference for a particular whisker cortical column, due to
232 the heterogeneity between clusters.

233 **D1 and D2 SPNs receive similar input from the barrel cortex**

234 Finally, we investigated whether innervation patterns differed between the two populations of SPNs,
235 expressing D1 or D2 receptors. Based on previous studies, unlabeled neurons in Drd1a-tdTomato
236 hemizygous mice were principally SPNs expressing the D2 receptor (Bertran-Gonzalez et al., 2008; Ade
237 et al., 2011; Enoksson et al., 2012; Thibault et al., 2013; Cao et al., 2018). As previously reported (Wall et
238 al., 2013), projections to D1 and D2 SPNs were spatially intermingled along the axis of barrels (Fig. 6A,B ;
239 n = 47 and 54, cells respectively). We found that D1 and D2 SPNs had similar input fields: first, their

240 widths were not different (Fig. 6C). In addition, they received input from a similar number of cortical
241 columns, which were organized in clusters of similar widths (Fig. 6D,E). Paired analysis of D1 and D2
242 SPNs recorded in the same slice also showed that their input fields did not significantly differ in width,
243 number of cortical columns or cluster width (p = 0.44 – 0.50 – 0.26, Wilcoxon; Fig. 6C-E). None of these
244 parameters exhibited a clear relationship between subtypes (R = 0.13 – 0.30 – -0.003; p = 0.43 – 0.058 –
245 0.99, Pearson; Fig. 6C-E). Finally, both types of SPNs received input from each cortical layer in similar
246 proportions (Fig. 6F). Thus, the heterogeneity in patterns of innervation is not due to a difference
247 between SPN subtypes. Overall, there was no difference in the total inputs received by D1 and D2 SPNs
248 (EPSC sum or $EPSC^T$; Fig. 6G). In addition, the principal cluster was similarly dominant over the other
249 clusters (Fig. 6H). However, differences were observed in a layer-specific manner (Fig. 6I). Whereas L5-
250 $EPSC^T$ was similar in D1 and D2 cells, differences were found in L2/3 and L6: L2/3-$EPSC^T$ was larger in D2
251 SPNs (132 ± 36 vs. 53 ± 22 pA, p = 0.005, Mann-Whitney) but L6-$EPSC^T$ was larger in D1 SPNs (37 ± 10 vs.
252 16 ± 2 pA, p = 0.038). Further analysis suggested a difference in the strength of synapses as principal
253 mechanism. Indeed, L2/3-EPSCs evoked at single sites were larger in D2 SPNs (48 ± 11 pA vs. 27 ± 5 pA;
254 p = 0.043) whereas L6-EPSCs were larger in D1 SPNs (24 ± 2 pA vs. 16 ± 2 pA ; p = 0.038).

255 Discussion

256 We investigated the organization of functional projections originating in the barrel cortex and targeting
257 projection neurons in the dorsal striatum in a novel preparation. We found overall little input
258 convergence as cortical neurons innervating an SPN were either located in a single cortical column or
259 thinly scattered across the barrel field. Each SPN had a distinct pattern of innervation from the barrel
260 cortex, albeit with occasional overlap for SPNs closely positioned in the DLS. D1 and D2 presented
261 similar patterns of innervations.

262 Sparse sensory innervation of single SPNs

263 As previously revealed by tracings of corticostriatal projections, the primary source of innervation of
264 SPNs in this study is the upper part of L5 in the barrel cortex, L5a, although, SPNs are occasionally
265 innervated by cells located in deeper and superficial layers (Wise and Jones, 1977; Reiner et al., 2003;
266 Wall et al., 2013; Guo et al., 2017; Yamashita et al., 2018; Bertero et al., 2022). Given the abundance of
267 cortical axons in the striatum, it has been assumed that a large number of cortical cells innervate each
268 SPN, potentially up to few thousands if synaptic connections were made promiscuously (Kincaid et al.,
269 1998). On the other hand, it has also been reported that neurons in the DLS fire in response to the

stimulation of a single body-part in monkeys and rodents *in vivo*, even of a single whisker in some cases (Carelli and West, 1991; Jaeger et al., 1995; Cho and West, 1997). This finding suggested that each striatal neuron was in fact innervated by one small subregion of S1, although feedforward inhibition could have masked a broader selectivity (Pidoux et al., 2011). Here, the LSPS connectivity maps indicate that convergence from the barrel cortex to individual SPNs is indeed low as 60 % of SPNs responded to the stimulation of only one or two whisker cortical columns present in the preparation. The LSPS combined with glutamate uncaging mapped projections contained in the slice, intact from the presynaptic cell bodies to the SPN dendrites. Some cortical inputs targeting distal SPN dendrites may have gone undetected, either due to attenuation of synaptic events recorded at the soma or because distal dendritic branches were lost during slice preparation. Indeed, about 80 % of S1 synaptic contacts are distributed along dendrites (Sanabria et al., 2024). However, synapses located distally are proportionally rare (Sanabria et al., 2024), and our estimates suggest that the loss of S1 input was minimal (see Methods). More significantly, our mapping only included projections from neuronal somata located within the S1 barrel field in the slice: projections from cortical columns outside the slice were not stimulated. For this reason, our study characterized connectivity patterns rather than the full extent of connectivity with the barrel cortex**.** A number of critical findings argue that innervation on individual SPNs is genuinely sparse: i) The cortical columns present in the slice corresponded to different whisker arcs, an axis associated with the greatest overlap of cortical axons in the striatum (Alloway et al., 1999), and therefore where input convergence could have been high. This organization was visible in the global SPN LSPS connectivity map (Fig. 2J). ii) The peak of connectivity was with L5a as previously documented, not with a layer closer to striatum, as this would be the case if the native organization of the projection was altered in the preparation. iii) The connected sites were scattered along broad horizontal and vertical axes, implying that projections in between were preserved. Critically, the fact that adjacent SPNs had different connectivity patterns in the same slice further supported the presence of a pool of potential connections larger than the number of actual connections made on each SPN. iv) Connectivity clusters were sparser in larger input fields, suggesting that the number of presynaptic cells to an SPN was regulated and reached a plateau. v) EPSCs were small, consistent with one or a few presynaptic cells at each connected site. Altogether, our results support the model in which, within a loosely topographical organization of projections, each SPN integrates limited and heterogeneous rather than exhaustive inputs transmitted by the barrel cortex (Fig. 7). The speckled connectivity pattern of individual SPNs, arising from the abundant and diffuse cortical innervation in the DLS, suggests that somatosensory corticostriatal synapses are established through a selective and/or competitive process.

302 It is important to determine whether this sparse innervation of SPNs by S1 is a characteristic shared with
303 other projections. In particular, it will be interesting to test this hypothesis on the auditory projections
304 targeting the posterior striatum, where neurons exhibit clear tone frequency selectivity (Guo et al.,
305 2018).

306 **Specific cortical input to individual SPNs**

307 A peculiar feature of the corticostriatal innervation is the imbalance between the number of cortical
308 cells projecting to the striatum and the number of striatal cells, thought to be at a ratio of 10 to 1
309 (Oorschot, 1996). Based on this ratio and the ultrastructure of the corticostriatal connection, the density
310 of axonal boutons and spines, C. Wilson's group concluded that the probability of an SPN being
311 contacted by one given axon entering the domain of its dendritic arborization was low, 0.04 - 1.4 %,
312 depending on the model. Hence, the chance that two SPNs were innervated by the same cortical axon
313 was even lower according to this model. Consistent with it, here, we found that overlaps between the
314 connectivity maps of SPNs were rare and, when present, involved only a small fraction of the connected
315 sites. This indicates that neighboring SPNs predominantly integrated distinct inputs from the barrel
316 cortex, although it is possible that overlapping inputs received in distal dendrites were not all detected.
317 Overlaps occurred only for SPNs located within 250 µm of each other. In contrast, input fields continued
318 to intersect significantly beyond 250 µm and up to 500 µm of separation between SPNs. This means that
319 relatively distant SPNs could share a general region of connectivity in the barrel cortex without any of
320 their presynaptic partners residing within the same cortical column. Interestingly, the observation that
321 two SPNs must be less than 250 µm apart to share some of their inputs was not predicted by the known
322 ultrastructure of corticostriatal connections. In fact, it predicted the opposite: that two SPNs would
323 more likely to be innervated by the same cortical cell if their dendrites extended into different striatal
324 subregions, as this would increase the likelihood of each SPN contacting boutons of this cortical cell, as
325 these are sparsely distributed in the striatum (Kincaid et al., 1998). One possible explanation for this
326 discrepancy could be that, in our experiments, pairs of SPNs with shared connectivity were innervated
327 by different neurons that were co-localized in the barrel cortex (< 75 µm apart). Such events could also
328 be at the origin of the striatal clusters described *in vivo,* in which neurons had similar, yet non-identical,
329 sensory selectivity (Carelli and West, 1991; Jaeger et al., 1995).

330 **Similarities and specificities in the patterns of projection to SPNs of the direct and indirect pathways**

331 Electrophysiological studies have shown that D1 SPNs exhibit larger responses than D2 SPNs to whisker
332 deflections (Reig and Silberberg, 2014; Filipović et al., 2019). Also, the optostimulation of cortical

efferents in brain slices showed a bias towards D1 SPNs (Kress et al., 2013; Parker et al., 2016). In our study, we had contrasting results. There was no difference in the innervation of D1 and D2 SPNs, neither in the rate at which cells were connected by layers, nor in the organization of the projection. The principal layer innervating SPNs, L5a, delivered inputs of similar strengths to D1 and D2 SPNs. However, layers with lower incidence in the pattern of innervation showed bias in the amplitude of responses: stimulations in L2/3 induced stronger responses in D2 cells whereas stimulations in L6 activated D1 cells more strongly. We have shown that stimulation in L2/3 activates the L2/3 projection only. Similarly, the L6-evoked EPSCs are consistent with the axon collaterals that L6 corticofugal projection neurons have in the striatum (Guo et al., 2017; Bertero et al., 2022). The larger L2/3 inputs received by the D2 SPNs is intriguing because of the role of this layer in higher-order integration processes, such as those activated during operant sensory discrimination tasks (Kwon et al., 2016; Han and Helmchen, 2024; Oryshchuk et al., 2024). Moreover, the activity of L2/3 cells during mouse displacement is distinctive, exhibiting a sustained response to ongoing whisker-wall contacts, as opposed to the transient response observed in L5 (Ayaz et al., 2019). In L6, the population of corticofugal projection neurons is diverse, with some responding to whisking and sensory stimuli, while others are active during transitions into quiet periods of behavior (Dash et al., 2022; Vélez-Fort et al., 2014). Further investigation is needed to specifically examine projections from the upper and lower cortical layers and how they influence the dynamics of sensory integration in the direct and indirect pathways of the DLS. However, these data illustrate the diversity of paths of sensory integration involving D1 and D2 SPNs.

In conclusion, we found a low and sparse connectivity within the cortical vibrissal projections to individual SPNs. While projections respected a loose topography, the innervation patterns of individual SPNs displayed substantial connectivity gaps and heterogeneity. Since the inputs to a single SPN represent only a limited subset of whisker columns, a complete representation of whiskers could emerge at the population level, with each SPN's representation complementing those of its neighbors (Fig. 7). These observations raise the hypothesis of a selective or competitive process underlying the formation of corticostriatal synapses. The degree of input convergence onto SPNs could be modulated by plasticity, potentially enabling experience-driven reconfiguration of S1 corticostriatal coupling.

361 # Materials and Methods

362 **Animals and ethics**

363 Hemizygous male and female B6.Cg-Tg(Drd1a-tdTomato)6Calak/J mice (JAX stock #016204; Ade et al.,
364 2011) were used on postnatal day 22-43, in accordance with institutional guidelines and the French
365 Ministry of Research (APAFIS#27242).

366 **Brain slices preparation and electrophysiology.**

367 Mice were deeply anesthetized with isoflurane (4 %) prior to cervical dislocation and decapitation. We
368 prepared corticostriatal slices (350 µm thick) from the brain left hemisphere, based on stereotaxic
369 coordinates placing the striatal cells 1-2 mm anteriorly to the projection neurons in the barrel cortex
370 (Aronoff et al., 2010; de la Torre-Martinez et al., 2023). Parasagittal slices were cut with a 60° angle from
371 the midline and a 10° angle in the dorso-ventral axis (Supplemental Fig. 1A) in a chilled cutting solution
372 containing (in mM): 110 choline chloride, 25 NaHCO3, 25 D-glucose, 11.6 sodium ascorbate, 7 MgCl2,
373 3.1 sodium pyruvate, 2.5 KCl, 1.25 NaH2PO4, and 0.5 CaCl2 (Sigma Aldrich). Slices were then transferred
374 to artificial cerebrospinal fluid (ACSF) containing (in mM): 127 NaCl, 25 NaHCO3, 25 D-glucose, 2.5 KCl, 1
375 MgCl2, 2 CaCl2, and 1.25 NaH2PO4, aerated with 95% O2/5% CO2. Slices were first incubated at 34 °C
376 for 30 min and then maintained at room temperature for 20 min prior to use. Slices used for LSPS (1-2
377 per animal) contained barrels in the L4 of cortex, the globus pallidus, its external segment (GPe), the
378 internal capsule, the ventral posteromedial nucleus of thalamus and the anterior hippocampus. ~ 8
379 barrels (5-13) were visible in the slice. 2 rows of barrels may have been superimposed. At the end of
380 each experiment, a picture of the slice was saved in order to superimpose it digitally to other slices,
381 according to visual landmarks (Adobe Photoshop; Adobe Inc.). SPNs were visualized under infrared and
382 fluorescent lights in a BX61WI microscope (Olympus) and patched with borosilicate electrodes (3–6 MΩ)
383 and recorded in the voltage-clamp whole-cell configuration using a Multiclamp 700A amplifier (Axon
384 Instrument, Molecular Devices). The holding membrane potential was – 80 mV. The intracellular
385 solution contained (in mM) 128 Cs-methylsulfate, 4 MgCl2, 10 HEPES, 1 EGTA, 4 Na2ATP, 0.4 Na2GTP, 10
386 Na-phosphocreatine, 3 ascorbic acid; pH 7.25; 290-300 mOsm. Cells in L5 and L2/3 of the barrel cortex
387 were recorded in the current-clamp mode, with an intracellular solution in which Cs-methylsulfate was
388 replaced by K-methylsulfate. All experiments were performed at room temperature (21°C).

389 **LSPS with glutamate uncaging**

390 LSPS was performed as described previously (Bureau et al., 2006). Recirculating (2 mL/min) ACSF
391 solution contained (in mM): 0.2 MNI-caged glutamate (Tocris), 0.005 CPP [()-3-(2-carboxypiperazin-4-yl)

392 propyl-1-phosphonic acid], 4 $CaCl_2$, and 4 $MgCl_2$. Focal photolysis of caged glutamate was accomplished
393 with a 2 ms 20 mW pulse of a pulsed UV (355 nm) laser (DPSS Lasers Inc.) through a 0.16 NA 4 ×
394 objective (Olympus). 25 mW laser pulses were used for stimulating cortical neurons in mice older than
395 P30 to maintain their excitation at a similar level than in younger mice (Supplemental Fig. 2B). The
396 stimulus pattern for mapping the corticostriatal projections was 464 positions spaced by 75 µm on a 29
397 × 16 grid (2.1 × 1.1 mm) over barrel cortex. The corticostriatal slice and the LSPS grid were oriented in
398 such a way that layer 5a was laid out horizontally. UV stimuli were applied every 700 ms and their
399 successive positions on the LSPS grid were such as to maximize the time between stimulations of
400 neighboring sites. Electrophysiological traces consisted of 100 ms baseline, a 450 ms window followed
401 by a -5 mV 100 ms test pulse. A minimum of 2 and up to 4 stimulations were performed at each site at
402 several minutes intervals. Custom software for instrument control and acquisition (Suter et al. 2010)
403 was written in Matlab (Mathworks). Excitation profiles of pyramidal neurons were generated under
404 similar conditions except that cells were recorded in current-clamp mode and glutamate was uncaged
405 on a smaller 8 × 8 grid covering their soma and dendrites (50 µm spacing; 350 × 350 µm). In a subset of
406 L5a cell recordings, a 8 × 24 grid was used to stimulate up in L1 (50 µm spacing).

407 **Analysis of LSPS data**

408 Synaptic input maps of neurons were constructed by taking the peak amplitude of EPSCs detected in a
409 50 ms time window starting at stimulation onset for each position in the LSPS grid. Measures were
410 averaged across repetitions of stimulations (2-4). The threshold for EPSC detection was 3 standard
411 deviations from baseline, or 9.2 ± 0.4 pA. To disambiguate evoked responses from spontaneous activity,
412 synaptic responses occurring less than 2 times across repetitions of maps were set to zero. Averaged
413 maps were superimposed taking L5a as reference in the vertical axis and the junction of the GPe, dorsal
414 striatum and internal capsule as reference in the horizontal axis (Ref_{hor}). In order to detect connectivity
415 clusters and center of mass in the LSPS map, we used the binary version of the map ('connectivity map')
416 reporting the location of connected and non-connected sites (i.e., yielding EPSCs or none in the
417 recorded SPN). To detect clusters, the binary map was collapsed along its vertical axis. A cluster
418 comprised 1 or more consecutive connected sites that was framed by 1 or more non-connected sites.
419 Thus, a cluster here may include connected sites that were not adjacent on the vertical axis in the
420 original map, and may combine synaptic inputs from different layers. The number of cortical columns
421 was estimated based on the number of consecutive connected sites (ConsSites) in the collapsed map
422 and the mean width of a barrel in the slice, 150 µm, which is equal to 2 connected sites in the map.

423 Hence, the number of cortical columns = Σ (ceiling(ConsSites/2)). The connectivity center of mass was
424 computed based on the uncollapsed map as follows : Σ (Σ_{vert} connected sites × lateral distance from
425 Ref_{hor}) /Σ (Σ_{vert} connected sites). The synaptic input center of mass was computed based on the original
426 map, after thresholding, as follows: Σ ($mean_{vert}$ EPSC × lateral distance from Ref_{hor}) /Σ ($mean_{vert}$ EPSC).
427 Traces from current clamp recordings were analyzed to count the number of action potentials (APs)
428 elicited upon glutamate uncaging. In the 8 × 8 grid, 50 µm spacing, total number of spikes was 2.2 ± 0.2
429 for L2/3 pyramidal cells (n = 26), 5.4 ± 0.6 for regular spiking (RS) pyramidal cells in L5a (n = 30) and 9.9
430 ± 1.6 for non-RS pyramidal cells in L5b (n = 10). The number of spikes elicited by uncaging at single sites
431 was 1 or 2 and on average: 1.04 ± 0.04 for L2/3 cells, 1.03 ± 0.02 for L5 RS cells and 1.04 ± 0.02 for L5
432 non-RS cells. As spacing in the stimulation grid was 50 µm in these particular experiments, we used the
433 following equation to compute the number of sites with AP (sAP) in a stimulation grid with a spacing of
434 75 µm (i.e. as in connectivity maps): $sAP_{75} = sAP_{50} \times (75/50)^2$**.** To estimate the loss of S1 synaptic contacts
435 caused by slice preparation, we modeled the SPN dendritic field as a sphere centered on the soma. S1
436 synapses were at 80 % distributed radially along dendrites, according to the specific distribution
437 described by Sanabria et al. (2024). The simulation also incorporated the known distribution of SPN
438 dendritic length as a function of distance from the soma (Gertler et al., 2008). Finally, it assumed that
439 synapse placement was isotropic, with equal probability in all directions from the soma. Truncation was
440 simulated by removing a spherical cap at one pole of the sphere, reflecting the depth of our recordings
441 (beyond 80 µm). Based on this simulation, the loss of S1 inputs was < 10 %.

442 **Labeling of cortical cells**

443 In a somatosensory corticostriatal slice prepared as described above, biocytin (2 %) was injected by
444 iontophoresis in the L5a through a patch electrode (200 ms, 2.5 Hz) for 2 x 10 minutes (Chang, LoTurco
445 and Nisenbaum, 2000). The slice was incubated for 4 hours at room temperature in ACSF and
446 transferred to 4 % paraformaldehyde at 4°C overnight. It was rinsed in PBS containing 0.3 % Triton X-100
447 (PBS-T), incubated overnight at room temperature in streptavidin-AlexaFluor488 (1:1000 in PBS-T) and
448 mounted using Vectashield mount medium. Image acquisition was performed using a LSM 800 confocal
449 Zeiss microscope.

450 **Statistical analysis**

451 All data are expressed as mean ± SEM in the text. Median and 25-75th percentiles are shown in Figures.
452 N and n are the numbers of animals and neurons, respectively. Unless stated otherwise, paired or
453 unpaired non parametric tests, and Kruskal-Wallis test for repeated measures followed by Dunn post-

hoc test and Šidák correction for multiple comparisons were used. $p < 0.05$ is considered as statistically significant.

Acknowledgments:
This work was supported by funding from the Institut National de la Santé et de la Recherche Médicale and grants from the Agence Nationale de la Recherche (Corticostriatal, ANR-20-CE16-0002; STEP, ANR-20-CE17-0025-01). K. Amroune is supported by fellowships from the Ministère de l'Enseignement Supérieur et de la Recherche, from the governmental "France 2030" program via A*Midex (Initiative d'Excellence d'Aix-Marseille Université, AMX-19-IET-004) and by ANR funding (ANR-17-EURE-0029). L. Fontolan is supported by funding from Excellence Initiative of Aix Marseille Université - A*MIDEX (Turing Centre for Living Systems). We thank the staff of the animal and genotyping facilities, the histology and imaging platforms of INMED, the members of the CBGB group and Antoine Depaulis for their help and support. We thank Elodie Fino, Rosa Cossart, Ede Rancz, Roustem Khazipov, Thomas Morvan, Jean-Luc Gaiarsa, Corinne Beurrier and Lydia Kerkerian Le Goff for their critical reading of the manuscript.

References

Ade KK, Wan Y, Chen M, Gloss B, Calakos N (2011) An Improved BAC Transgenic Fluorescent Reporter Line for Sensitive and Specific Identification of Striatonigral Medium Spiny Neurons. Front Syst Neurosci 5:32.

Adibi M (2019) Whisker-Mediated Touch System in Rodents: From Neuron to Behavior. Front. Syst. Neurosci 13:40.

Alloway KD, Crist J, Mutic JJ, Roy SA (1999) Corticostriatal Projections from Rat Barrel Cortex Have an Anisotropic Organization that Correlates with Vibrissal Whisking Behavior. J Neurosci 19:10908–10922.

Alloway KD, Mutic JJ, Hoffer ZS, Hoover JE (2000) Overlapping corticostriatal projections from the rodent vibrissal representations in primary and secondary somatosensory cortex. J Comp Neurol 428:51–67.

Aronoff R, Matyas F, Mateo C, Ciron C, Schneider B, Petersen CCH (2010) Long-range connectivity of mouse primary somatosensory barrel cortex. Eur J Neurosci 31:2221–2233.

Ayaz A, Stäuble A, Hamada M, Wulf M-A, Saleem AB, Helmchen F (2019) Layer-specific integration of locomotion and sensory information in mouse barrel cortex. Nat Commun 10:2585.

Benison AM, Ard TD, Crosby AM, Barth DS (2006) Temporal patterns of field potentials in vibrissa/barrel cortex reveal stimulus orientation and shape. J Neurophysiol 95:2242–2251.

Bertero A, Verrillo L, Apicella AJ (2022) A Novel Layer 4 Corticofugal Cell Type/Projection Involved in Thalamo-Cortico-Striatal Sensory Processing. J Neurosci 42:1383–1405.

487 Bertran-Gonzalez J, Bosch C, Maroteaux M, Matamales M, Hervé D, Valjent E, Girault J-A (2008)
488 Opposing patterns of signaling activation in dopamine D1 and D2 receptor-expressing striatal
489 neurons in response to cocaine and haloperidol. J Neurosci 28:5671–5685.

490 Braitenberg V, Schüz A (1998) Cortex: Statistics and Geometry of Neuronal Connectivity. Springer

491 Bureau I, Shepherd GMG, Svoboda K (2008) Circuit and plasticity defects in the developing
492 somatosensory cortex of FMR1 knock-out mice. J Neurosci 28:5178–5188.

493 Bureau I, von Saint Paul F, Svoboda K (2006) Interdigitated paralemniscal and lemniscal pathways in the
494 mouse barrel cortex. Plos Biol 4:e382

495 Cao J, Dorris DM, Meitzen J (2018) Electrophysiological properties of medium spiny neurons in the
496 nucleus accumbens core of prepubertal male and female Drd1a-tdTomato line 6 BAC transgenic
497 mice. J Neurophysiol 120:1712–1727.

498 Carelli RM, West MO (1991) Representation of the body by single neurons in the dorsolateral striatum of
499 the awake, unrestrained rat. J Comp Neurol 309:231–249.

500 Cepeda C, Andre VM, Yamazaki I, Wu N, Kleiman-Weiner M, Levine MS (2008) Differential
501 electrophysiological properties of dopamine D1 and D2 receptor-containing striatal medium-
502 sized spiny neurons Eur J Neurosci 27:671-682

503 Chang SL, LoTurco JJ and Nisenbaum LK (2000) In vitro biocytin injection into perinatal mouse brain: a
504 method for tract tracing in developing tissue. J Neurosci Methods 97:1-6

505 Cho J, West MO (1997) Distributions of single neurons related to body parts in the lateral striatum of the
506 rat. Brain Res 756:241–246.

507 Cowan RL, Wilson CJ (1994) Spontaneous firing patterns and axonal projections of single corticostriatal
508 neurons in the rat medial agranular cortex. J Neurophysiol 71:17–32.

509 Dash S, Autio DM, Crandall SR (2022) State-Dependent Modulation of Activity in Distinct Layer 6
510 Corticothalamic Neurons in Barrel Cortex of Awake Mice. J Neurosci 42:6551-6565

511 Dehorter N, Michel FJ, Marissal T, Rotrou Y, Matrot B, Lopez C, Humphries MD, Hammond C (2011)
512 Onset of pup locomotion coincides with loss of NR2C/D-mediated cortico-striatal EPSCs and
513 dampening of striatal network immature activity. Front Cell Neurosci 5:24

514 de la Torre-Martinez R, Ketzef M, Silberberg G (2023) Ongoing movement controls sensory integration in
515 the dorsolateral striatum. Nat Commun 14:1004.

516 Enoksson T, Bertran-Gonzalez J, Christie MJ (2012) Nucleus accumbens D2- and D1-receptor expressing
517 medium spiny neurons are selectively activated by morphine withdrawal and acute morphine,
518 respectively. Neuropharmacology 62:2463–2471.

519 Erlandson MA, Manzoni OJ, Bureau I (2015) The Functional Organization of Neocortical Networks
520 Investigated in Slices with Local Field Recordings and Laser Scanning Photostimulation. Plos One
521 10:e0132008.

522 Filipović M, Ketzef M, Reig R, Aertsen A, Silberberg G, Kumar A (2019) Direct pathway neurons in mouse
523 dorsolateral striatum in vivo receive stronger synaptic input than indirect pathway neurons. J
524 Neurophysiol 122:2294–2303.

525 Flaherty AW, Graybiel AM (1991) Corticostriatal transformations in the primate somatosensory system.
526 Projections from physiologically mapped body-part representations. J Neurophysiol 66:1249–
527 1263.

528 Flaherty AW, Graybiel AM (1994) Input-output organization of the sensorimotor striatum in the squirrel
529 monkey. J Neurosci 14:599–610.

530 Gertler TS, Chan CS, Surmeier DJ (2008) Dichotomous Anatomical Properties of Adult Striatal Medium
531 Spiny Neurons J Neurosci 28: 10814-10824

532 Guo C, Peng J, Zhang Y, Li A, Li Y, Yuan J, Xu X, Ren M, Gong H, Chen S (2017) Single-axon level
533 morphological analysis of corticofugal projection neurons in mouse barrel field. Sci Rep 7:2846.

534 Guo L, Walker WI, Ponvert ND, Penix PL, Jaramillo S (2018) Stable representation of sounds in the
535 posterior striatum during flexible auditory decisions. Nat Commun 9:1534

536 Han S, Helmchen F (2024) Behavior-relevant top-down cross-modal predictions in mouse neocortex. Nat
537 Neurosci 27:298-308

538 Hooks BM, Papale AE, Paletzki RF, Feroze MW, Eastwood BS, Couey JJ, Winnubst J, Chandrashekar J,
539 Gerfen CR (2018) Topographic precision in sensory and motor corticostriatal projections varies
540 across cell type and cortical area. Nat Commun 9:3549.

541 Jaeger D, Gilman S, Aldridge JW (1995) Neuronal activity in the striatum and pallidum of primates
542 related to the execution of externally cued reaching movements. Brain Res 694:111–127.

543 Kincaid AE, Zheng T, Wilson CJ (1998) Connectivity and Convergence of Single Corticostriatal Axons. J
544 Neurosci 18:4722.

545 Kravitz AV, Freeze BS, Parker PRL, Kay K, Thwin MT, Deisseroth K, Kreitzer AC (2010) Regulation of
546 parkinsonian motor behaviours by optogenetic control of basal ganglia circuitry. Nature
547 466:622–626.

548 Kreitzer AC, Malenka RC (2007) Endocannabinoid-mediated rescue of striatal LTD and motor deficits in
549 Parkinson's disease models. Nature 445:643-647

550 Kress GJ, Yamawaki N, Wokosin DL, Wickersham IR, Shepherd GMG, Surmeier DJ (2013) Convergent
551 cortical innervation of striatal projection neurons. Nat Neurosci 16:665–667.

552 Kwon SE, Yang H, Minamisawa G, O'Connor DH (2016) Sensory and decision-related activity propagate in
553 a cortical feedback loop during touch perception. Nat Neurosci 19:1243–1249.

554 Mallet N, Le Moine C, Charpier S, Gonon F (2005) Feedforward inhibition of projection neurons by fast-
555 spiking GABA interneurons in the rat striatum in vivo. J Neurosci 25:3857–3869.

556 Oorschot DE (1996) Total number of neurons in the neostriatal, pallidal, subthalamic, and substantia
557 nigral nuclei of the rat basal ganglia: a stereological study using the cavalieri and optical disector
558 methods. J Comp Neurol 366:580–599.

559 Oryshchuk A, Sourmpis C, Weverbergh J, Asri R, Esmaeili V, Modirshanechi A, Gerstner W, Petersen CCH,
560 Crochet S (2024) Distributed and specific encoding of sensory, motor, and decision information
561 in the mouse neocortex during goal-directed behavior. Cell Rep 43:113618.

562 Parker PRL, Lalive AL, Kreitzer AC (2016) Pathway-Specific Remodeling of Thalamostriatal Synapses in
563 Parkinsonian Mice. Neuron 89:734–740.

564 Peixoto RT, Wang W, Croney DM, Kozorovitskiy Y, Sabatini BL (2016) Early hyperactivity and precocious
565 maturation of corticostriatal circuits in Shank3B−/− mice. Nat Neurosci 19:716-724

566 Pennartz CMA, Berke JD, Graybiel AM, Ito R, Lansink CS, van der Meer M, Redish AD, Smith KS, Voorn P
567 (2009) Corticostriatal Interactions during Learning, Memory Processing, and Decision Making. J
568 Neurosci 29:12831–12838.

569 Peters A (1979) Thalamic input to the cerebral cortex. Trends Neurosci 2:183–185.

570 Pidoux M, Mahon S, Deniau J-M, Charpier S (2011) Integration and propagation of somatosensory
571 responses in the corticostriatal pathway: an intracellular study *in vivo*: Sensory responses in the
572 corticostriatal pathway. J Physiol 589:263–281.

573 Ramaswamy S, Markram H (2015) Anatomy and physiology of the thick-tufted layer 5 pyramidal neuron.
574 Front Cell Neurosci 9:233.

575 Reig R, Silberberg G (2014) Multisensory integration in the mouse striatum. Neuron 83:1200–1212.

576 Reiner A, Jiao Y, Del Mar N, Laverghetta AV, Lei WL (2003) Differential morphology of pyramidal tract-
577 type and intratelencephalically projecting-type corticostriatal neurons and their intrastriatal
578 terminals in rats. J Comp Neurol 457:420–440.

579 Robbe D (2018) To move or to sense? Incorporating somatosensory representation into striatal
580 functions. Curr Opin Neurobiol 52:123-130

581 Sanabria BD, Baskar SS, Yonk AJ, Linares-Garcia I, Abraira VE, Lee CR, Margolis DJ (2024) Cell-Type
582 Specific Connectivity of Whisker-Related Sensory and Motor Cortical Input to Dorsal Striatum.
583 ENeuro 11:1

584 Shepherd GMG, Pologruto TA, Svoboda K (2003) Circuit analysis of experience-dependent plasticity in
585 the developing rat barrel cortex. Neuron 38:277–289.

586 Shepherd GMG, Svoboda K (2005) Laminar and columnar organization of ascending excitatory
587 projections to layer 2/3 pyramidal neurons in rat barrel cortex. J Neurosci 25:5670–5679.

588 Shepherd GMG, Stepanyants A, Bureau I, Chklovskii D, Svoboda K (2005) Geometric and functional
589 organization of cortical circuits. Nat Neurosci 8:782–790

590 Sippy T, Lapray D, Crochet S, Petersen CCH (2015) Cell-Type-Specific Sensorimotor Processing in Striatal
591 Projection Neurons during Goal-Directed Behavior. Neuron 88:298–305.

592 Smith Y, Bevan MD, Shink E, Bolam JP (1998) Microcircuitry of the direct and indirect pathways of the
593 basal ganglia. Neuroscience 86:353–387.

594 Suter BA, O'Connor T, Iyer V, Petreanu LT, Hooks BM, Kiritani T, Svoboda K, Shepherd GMG (2010)
595 Ephus: multipurpose data acquisition software for neuroscience experiments. Front Neural
596 Circuits 4:100

597 Thibault D, Loustalot F, Fortin GM, Bourque M-J, Trudeau L-É (2013) Evaluation of D1 and D2 Dopamine
598 Receptor Segregation in the Developing Striatum Using BAC Transgenic Mice. Plos One
599 8:e67219.

600 Vélez-Fort M, Rousseau CV, Niedworok CJ, Wickersham IR, Rancz EA, Brown APY, Strom M, Margrie TW
601 (2014) The stimulus selectivity and connectivity of layer six principal cells reveals cortical
602 microcircuits underlying visual processing. Neuron 83:1431-43

603 Wall NR, De La Parra M, Callaway EM, Kreitzer AC (2013) Differential innervation of direct- and indirect-
604 pathway striatal projection neurons. Neuron 79:347–360.

605 Wise SP, Jones EG (1977) Cells of origin and terminal distribution of descending projections of the rat
606 somatic sensory cortex. J Comp Neurol 175:129–157.

607 Wright AK, Norrie L, Ingham CA, Hutton EAM, Arbuthnott GW (1999) Double anterograde tracing of
608 outputs from adjacent “barrel columns” of rat somatosensory cortex. Neostriatal projection
609 patterns and terminal ultrastructure. Neuroscience 88:119–133.

610 Yamashita T, Vavladeli A, Pala A, Galan K, Crochet S, Petersen SSA, Petersen CCH (2018) Diverse Long-
611 Range Axonal Projections of Excitatory Layer 2/3 Neurons in Mouse Barrel Cortex. Front
612 Neuroanat 12:33.

613 Znamenskiy P, Zador AM (2013) Corticostriatal neurons in auditory cortex drive decisions during
614 auditory discrimination. Nature 497:482–485.

615

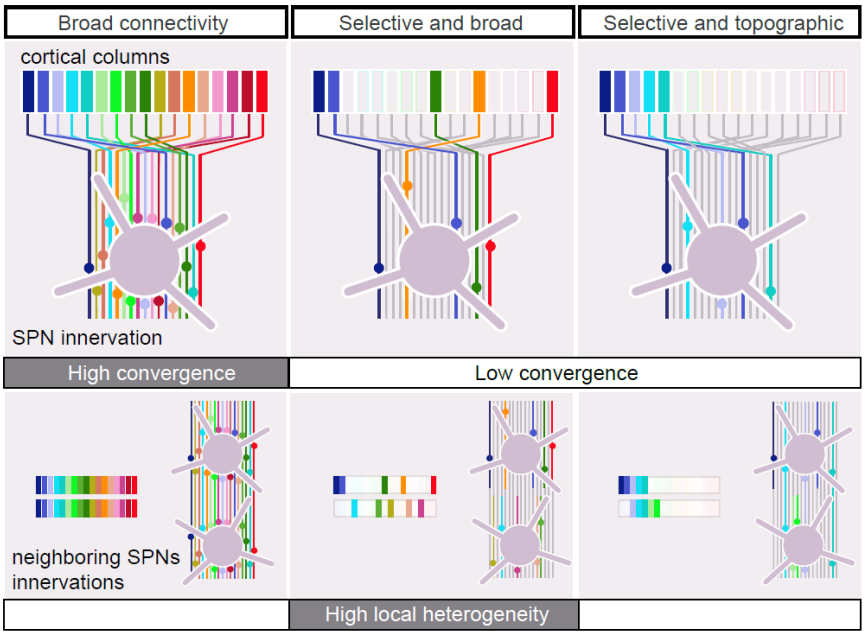

Figure 1. Potential connectivity patterns within the corticostriatal projection.
A rich and overlapping cortical innervation of the striatum (lines) permits different connectivity patterns: Left, synapses are formed promiscuously. In this case convergence is high as each SPN receives broad cortical input, from many cortical origins (colored bars on top). Middle and right, only a fraction of the potential connections are actually formed and, in these cases, convergence is lower. The selected presynaptic neurons are either scattered (middle) or topographically (right) positioned in the cortex. Increasing the selectivity of the corticostriatal connections while keeping their broad origin (middle) could generate maximal heterogeneity in the patterns of input for SPNs sharing the same striatal volume, due to a large number of combinations of cortical origins. In the case of a topographic innervation (right), neighboring SPNs form synapses with presynaptic neurons located in the same cortical region, reducing the local heterogeneity.

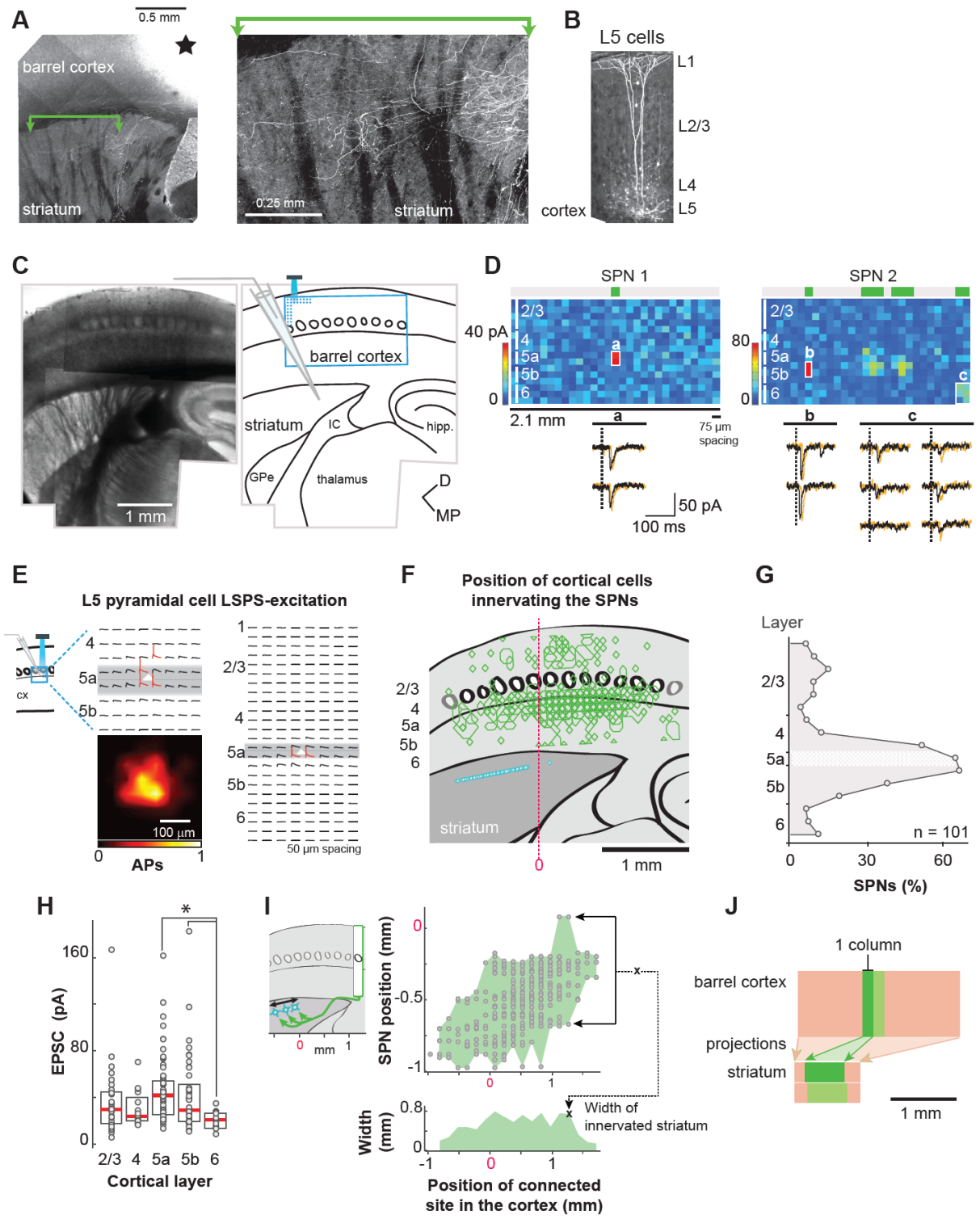

Figure 2. A novel slice preparation for investigating the spatial organization of the somatosensory projections to the DLS neurons.

A. A somatosensory corticostriatal slice in which axons from L5 neurons were labeled with biocytin iontophoresis. Black star, the electrode position in L5a. Right, focus on a region in the striatum.

B. Right, Example dendritic arbors of L5 cortical cells labeled with biocytin in the slice.
C. Montage of a corticostriatal slice (left) and layout of the experiment (right). A SPN was recorded in the dorsolateral striatum while cortical neurons were photostimulated with LSPS. The grid of LSPS (blue) was positioned on the barrel cortex. GPe, globus pallidus, external segment; IC, internal capsule; hipp., hippocampus.
D. Top, examples of synaptic input maps for individual SPNs showing one or four clusters of input (SPN 1 and 2, respectively). In the color maps, each pixel of color indicates the peak amplitude of EPSCs detected within a 50 ms window after the stimulus onset. The different cortical layers are represented by solid white vertical lines on the left side of the map. The green boxes at the top of the maps, the clusters of sites in the connectivity maps collapsed in the vertical axis whose stimulation evokes EPSCs. Bottom, EPSC traces evoked at the sites indicated by letters in the maps above. Two repetitions are superimposed (black and orange). Vertical dashed lines, the stimulus onsets (2 ms stimulus).
E. LSPS evoked excitation of two L5a pyramidal neurons recorded in current-clamp mode. LSPS was a 8 x 8 (left) or 24 x 8 (right) 50 µm spacing grid. Cortical neurons are positioned at the center (white triangles). Traces with an action potential are in red. Bottom, Average number of action potentials evoked at every site of the LSPS grid.
F. Overlay of the sites in the barrel cortex (green polygons) where stimulations evoked EPSCs in SPNs (cyan symbols; n =101 cells, N = 54 mice). The red dashed vertical line is the reference (Ref_{hor} in the Methods) used for aligning slices across experiments horizontally, on the junction of the striatum, GPe and IC .
G. Contribution of each cortical layer to the SPN innervations. The 16 rows of the grid correspond to different cortical layers (Layer 2/3: 1-6; L4: 7-9; L5a: 10; L5b: 11-13; L6: 14-16). The horizontal white band is L5a.
H. Amplitude of SPN EPSCs as a function of their laminar origin. Median (red) and 25-75th percentiles (boxes). * Kruskal-Wallis p = 0.000125, Dunn-Šidák posthoc tests, p = 0.0001 and 0.03415.
I. Top, Positions of SPNs in the striatum for each position of connected sites on the horizontal axis of the LSPS grid. Bottom, maximal distance between SPNs for every connected site position in the barrel cortex on the horizontal axis, binned every 150 µm, in other words the width of the projection zone of one cortical column within the striatum
J. Schematic of the slice with the size of the cortical and striatal regions that are connected by projections to SPNs (pink) and the size of the striatal domain with functional projections from a single cortical column (shades of green).

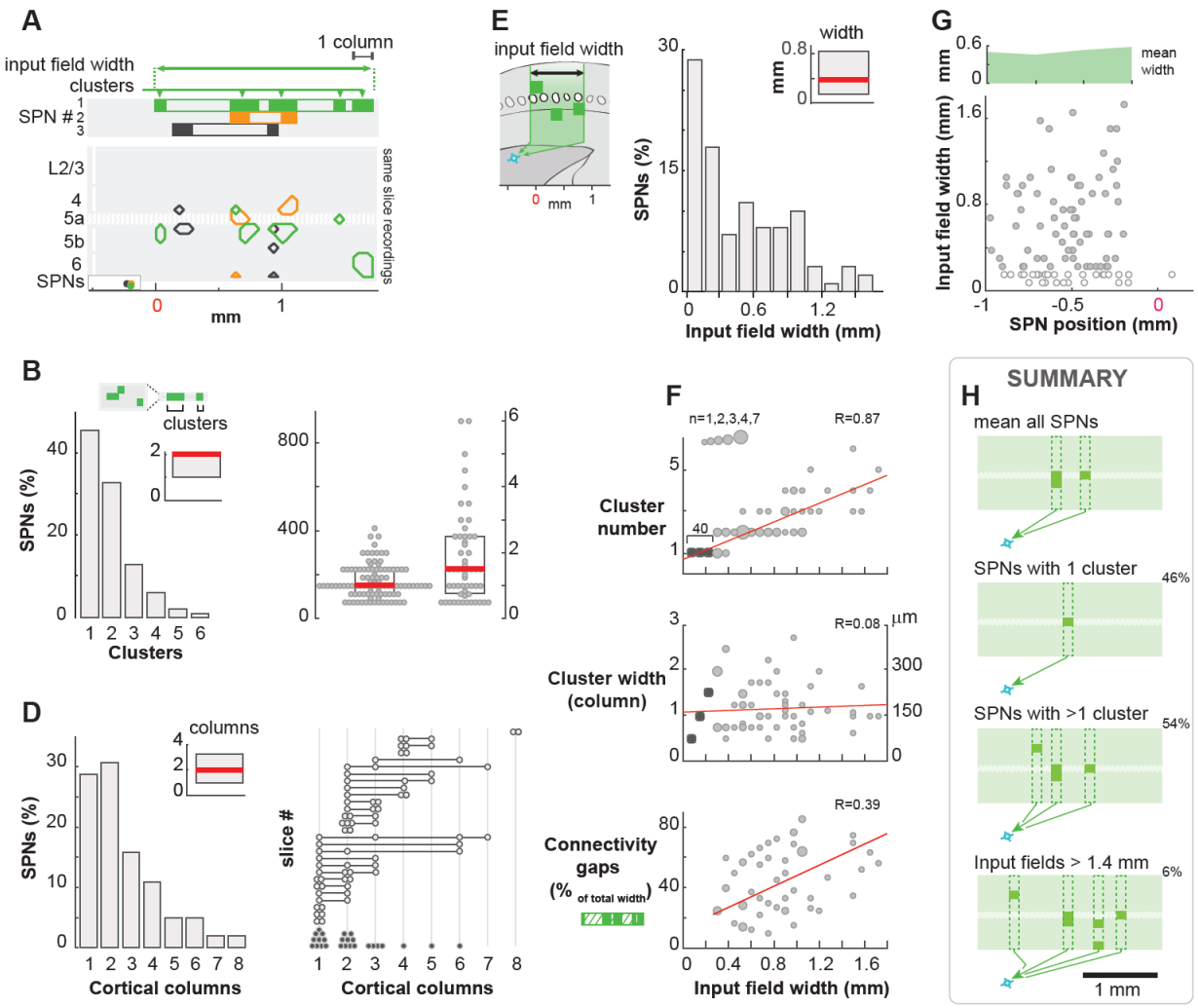

Figure 3. Sparse functional projections from the barrel cortex to individual SPNs in the DLS.
A. Example slice with 3 recordings. The hatched horizontal band is L5a, the polygons are the stimulation sites evoking EPSCs, the solid boxes on top are the connectivity clusters and the open rectangle the input field in the collapsed connectivity map. The circles at the bottom mark the positions of SPNs on the horizontal axis. Recordings are color coded.
B. Fraction of SPNs receiving inputs from 1 to 6 clusters of projections in the barrel cortex. In inset, median (red) and 25-75th percentiles (box). Clusters are defined as the ensemble of contiguous sites in the connectivity map collapsed in the vertical axis, whose stimulation evokes EPSCs (see examples in A, boxes at the top). n = 101 cells, N = 54 mice.
C. Median (red) and 25-75th percentiles (box) of cluster width and spacing, in µm (left Y axis) and in number of cortical columns (right Y axis).
D. Left, Fraction of cells receiving inputs from 1 to 8 cortical columns in the barrel area. In inset, median (red) and 25-75th percentiles (box). Right, Number of cortical columns innervating individual SPNs. Symbols are cells, lines are slices. Light gray symbols, slices with ≥ 2 recordings. Dark symbols, one recording per slice.

E. Fraction of SPNs with input fields from 0.075 to 1.6 mm.

F. Top to bottom, for every input field width, the number of clusters, the cluster's width (in number of cortical columns and in µm) and the percentage of the region without connected site in the input fields collapsed along the vertical axis. Gray symbols, cells with ≥ 2 connectivity clusters. Other symbols, cells with 1 cluster. Top to bottom, $p < 0.0001$, $p = 0.43$ and $p = 0.0031$ for the correlations.

G. Bottom, width of input fields in the barrel cortex for different positions of SPNs in the striatum. SPNs with an input field the size of a single or of several cortical columns are shown (open and solid symbols, respectively). Top, The average width of input fields as a function of SPN positions binned every 250 µm.

H. Schematized average and principal connectivity patterns. The % of SPNs is indicated for each pattern.

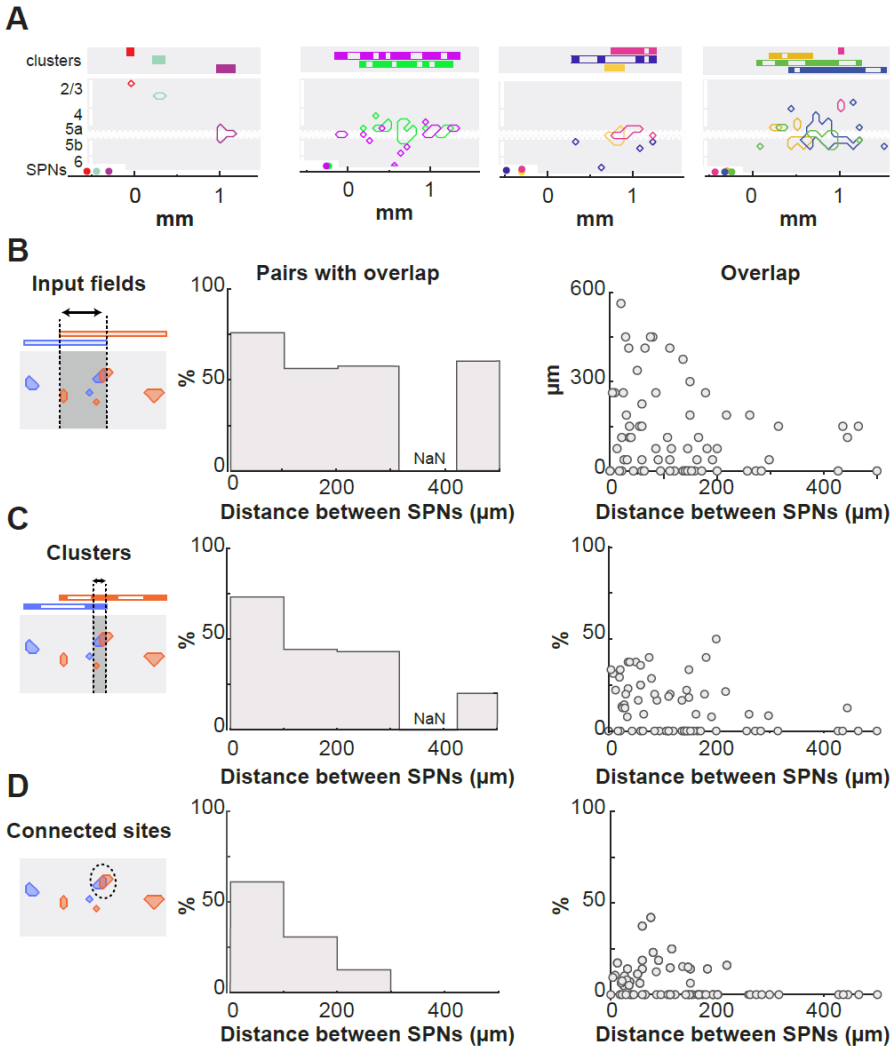

Figure 4. Individual SPNs have unique cortical innervation

A. Four example slices with 2 to 4 recordings. Same as in Fig. 3A.

B. Left, fraction of pairs with overlap in their input field. Right, width of overlap as a function of the horizontal distance separating cells. n = 70 pairs. NaN indicates the lack of data.

C. Same as in B for the fraction of vertical alignment between SPN connectivity maps.

D. Same as in B for the fraction of overlap between SPN connectivity maps.

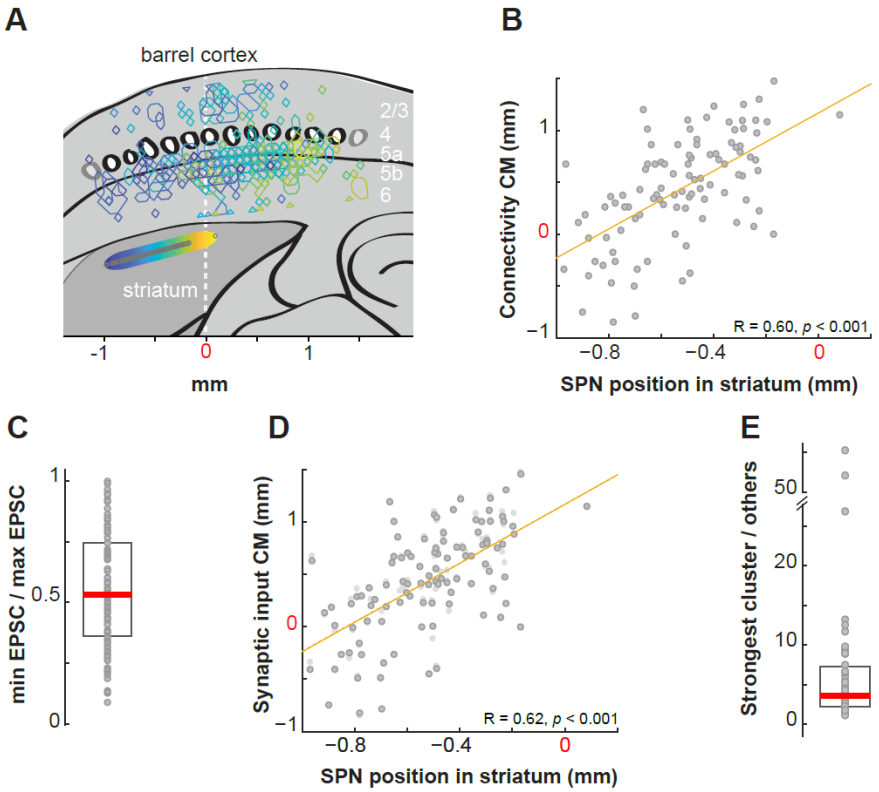

Figure 5. Topographic organization of the functional vibrissal innervation of SPNs in the DLS

A. Overlay of the sites in the barrel cortex where stimulations evoked EPSCs in SPNs. The colors, yellow to blue, indicate the position of the SPNs (gray circles) along the horizontal axis in the striatum (axis at the bottom, 0 is Ref_{hor} in the Methods; n = 101, N = 54). Blue shades are for lateral SPNs.

B. Position of the connectivity center of mass (CM) as a function of the SPN position in dorsal striatum. Zero on the x and y axis is the position of the vertical dashed line shown in A.

C. Ratio of the largest EPSC over the smallest EPSC for each recording. Median (red) and 25-75th percentiles (box).

D. Position of the synaptic input CM as a function of the SPN position in dorsal striatum. In light gray, the connectivity CM.

E. EPSC sum obtained in the strongest connectivity cluster relative to others sum. Cells with ≥ 2 clusters, n = 55.

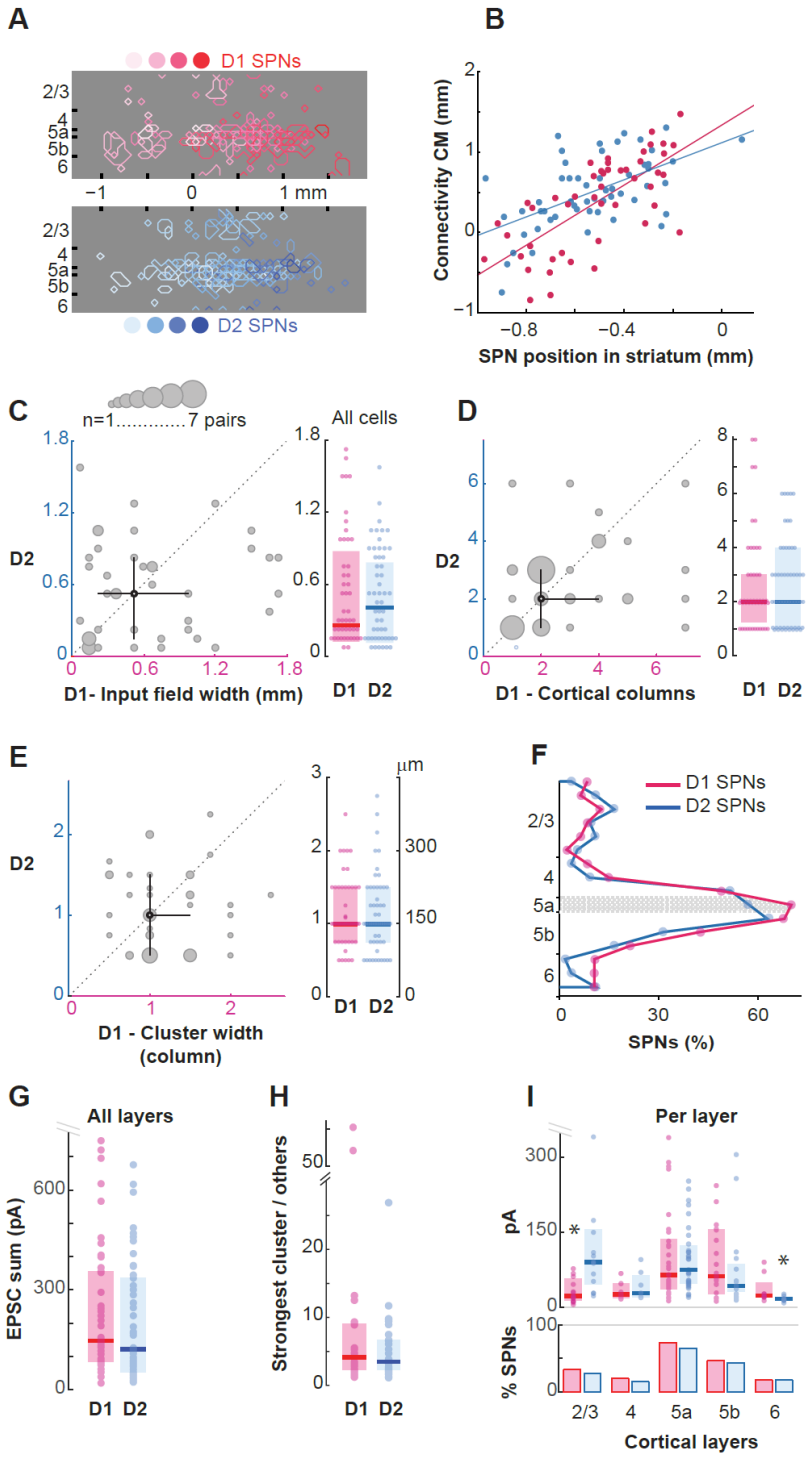

712

713 **Figure 6. D1 and D2 SPNs have similar patterns of innervation from the barrel cortex**

714 **A**. Overlay of the sites in the barrel cortex where stimulations evoked EPSCs in D1 (blue) or D2 SPNs
715 (red). The shades, dark to light, indicate the position of the SPNs (bottom circles) along the medio-lateral
716 axis in the dorsal striatum (axis at the bottom). D1 cells, n = 47, N = 36; D2 cells, n = 54, N = 37.

B. Position of the connectivity center of mass (CM) as a function of the SPN position in the dorsal striatum (D1, red; D2, blue). R = 0.70 (D1, n = 47, N = 36); R = 0.57 (D2, n = 54, N = 37).

C. Left, D2 SPN input field width as a function of the D1 SPN input field width, in the same slice. The black symbol and lines are the median value and 25-75th percentiles. Large symbols indicate n = 2 to 3 pairs. n = 42 pairs. Right, medians (thick lines) and 25-75th percentiles (boxes) of D1 and D2 input field widths, across all cells. n = 101.

D. Same as in C for the number of cortical columns.

E. Same as in C for the width of connectivity clusters.

F. Contribution of each cortical layer to the SPN innervations. The horizontal hatched band is L5a.

G. EPSC sum for D1 and D2 SPNs. Outliers were not shown for clarity (1 D1, 2 D2, 1.2-1.5 nA)

H. EPSC sum obtained from the strongest cluster relative to others. Cells with ≥ 2 clusters. D1, n = 24; D2, n = 30.

I. Top, D1 and D2 SPN EPSC sum as a function of laminar origin. For each layer, only cells with inputs are included. Outliers are not shown for clarity (3 D1, 2 D2, 350-700 pA). * indicates a significant difference (p = 0.005 and p = 0.008; Mann-Whitney). Bottom, fraction of cells with input.

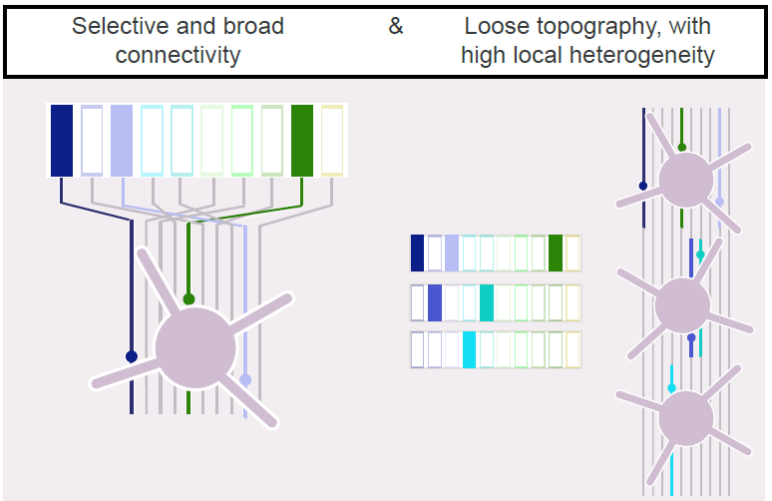

Figure 7. Connectivity pattern within the somatosensory corticostriatal projection to SPNs. Left, Our results support the model in which each SPN integrates limited and heterogeneous rather than exhaustive inputs transmitted by the barrel cortex, intermediate between the middle and right panels in Fig. 1. Right, Each SPN representation of the whisker cortical columns complements the representations of its neighbors.

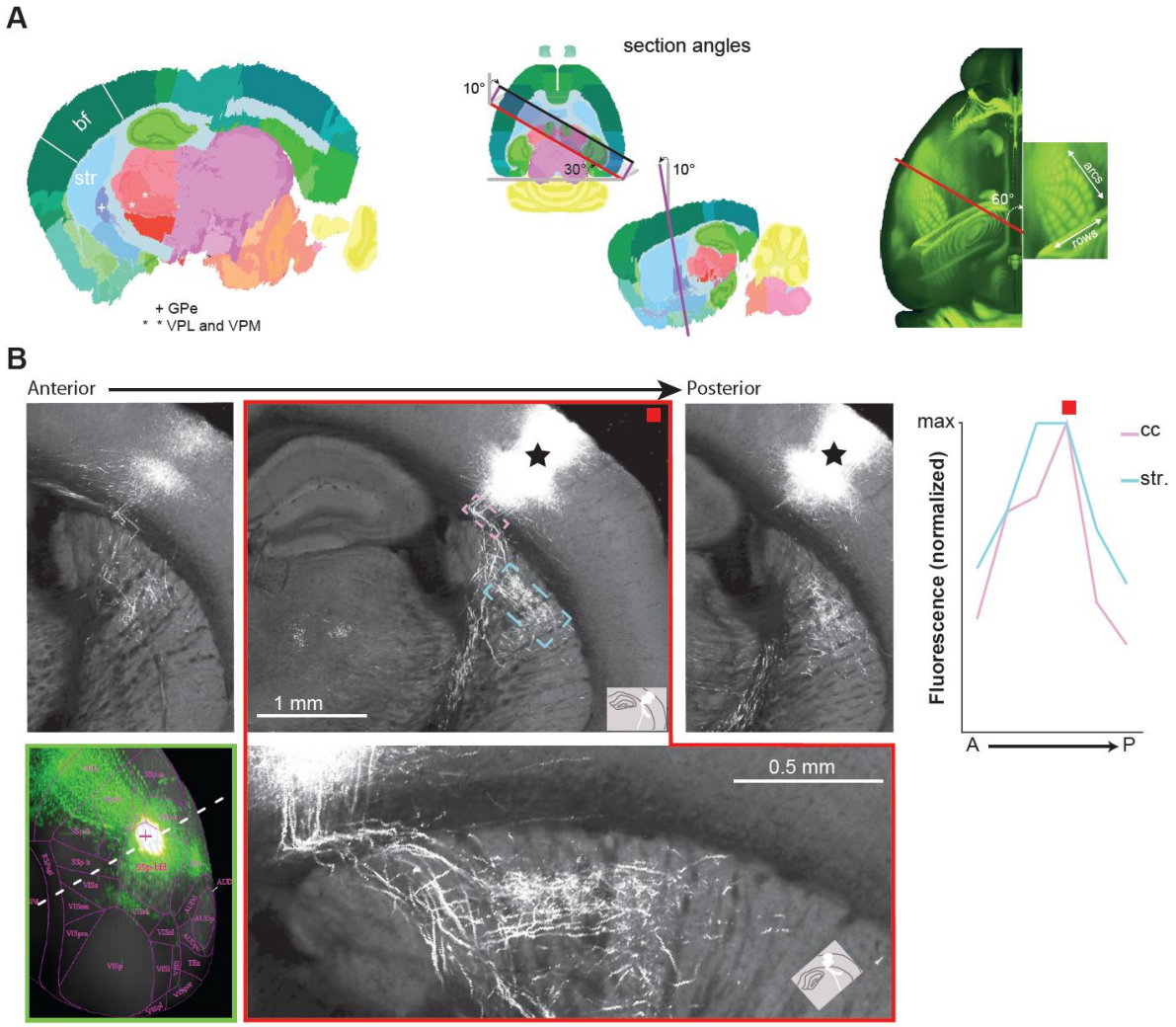

Supplemental Figure 1.

A. Left, the corticostriatal slice generated from the Allen mouse brain reference atlas (CutNII custom-angle slice visualization tool; G. Csucs). bf, barrel field. str, striatum. VPL, ventral posterolateral thalamic nucleus. VPM, ventral posteromedial thalamic nucleus. Center, the section angles illustrated on horizontal and longitudinal sections of the brain. Right, the section angle with respect to the orientations of the arcs and rows in the barrel field of the left hemisphere (Allen mouse brain atlas).

B. A simulated somatosensory corticostriatal slice generated using data from the Allen mouse connectivity atlas (https://connectivity.brain-map.org/projection/experiment/cortical_mp/293728197). eGFP was expressed in L2/3 and L5 pyramidal cells principally, in 3-4 arcs of the D and E rows of whisker columns (whole brain visualization in the green box at the bottom left; the dashed line indicates the slice orientation). Acquisitions of serial two-photon tomography were stacked in Fiji and the reconstituted brain was sectioned using the angles to produce the acute somatosensory corticostriatal slices (BigDataViewer plugging). The red box identifies the "experimental slice" with intact projections from the barrel cortex to the striatum. Fluorescence in the striatum (blue) and in the corpus callosum (cc, pink) was quantified on consecutive max projections (300 µm thick) obtained in the anterior-posterior

axis (A-P). Note that slices, being from the opposite hemisphere to our experiments, have the reverse orientation in the medio-lateral axis compared to Fig. 2A,C.

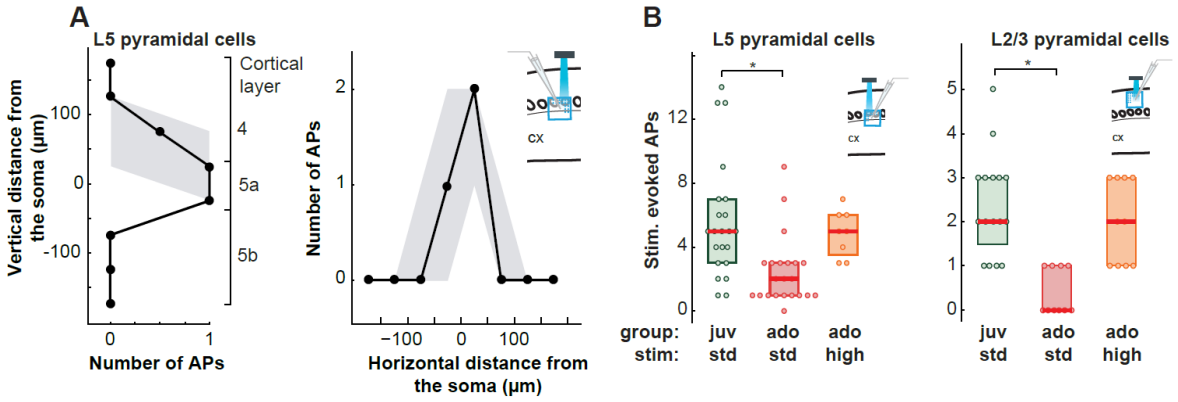

Supplemental Figure 2.

A. Vertical (left) and horizontal (right) excitation profile of L5 pyramidal cells recorded in current clamp, in the juveniles and adolescents combined (20 and 25 mW stimulation, respectively). Evoked action potentials (APs) were summed along each column (left) or line (right) of the LSPS grid (50 µm spacing). Solid line, median. In gray, 25-75th percentiles. n = 30, N = 14.

B. Total number of APs evoked in the stimulation grid for L5 (left) and L2/3 (right) pyramidal cells in juvenile (juv, P22-30) and adolescent (ado, P31-41) mice. A higher stimulation intensity was used for adolescent mice (25 mW instead of the standard -std - intensity, 20 mW), so that the total number of APs matched between the two age groups. L5, juv, n = 22, N = 9 ; ado std, n = 22, N = 13; ado high: n = 8, N = 5; L2/3, juv: n = 16, N=3; ado std and high n = 10, N = 2; * $p < 0.001$, Mann-Whitney.